

A MEASUREMENT OF THE ANGULAR POWER SPECTRUM OF THE MICROWAVE  
BACKGROUND MADE FROM THE HIGH CHILEAN ANDES

E. Torbet<sup>1</sup>, M. J. Devlin<sup>2</sup>, W. B. Dorwart<sup>1</sup>, T. Herbig<sup>1</sup>, A. D. Miller<sup>1</sup>, M. R. Nolte<sup>1</sup>, L.  
Page<sup>1</sup>, J. Puchalla<sup>2</sup>, H. T. Tran<sup>1</sup>

Draft 7 May 1999, to be submitted to Astrophysical Journal Letters

ABSTRACT

We report on a measurement of the angular spectrum of the anisotropy of the microwave sky at 30 and 40 GHz between  $l=50$  and  $l=200$  over 600 sq. deg. The data support a rise in the angular spectrum to a maximum with  $T_l \approx 85$  K at  $l=200$ . We also give a 2-sigma upper limit of  $T_l < 122$  K at  $l=432$  at 144 GHz. These results come from the first campaign of the Mobile Anisotropy Telescope (MAT) on Cerro Toco, Chile. To assist in assessing the site, we present plots of the fluctuations in atmospheric emission at 30 and 144 GHz.

Subject headings: cosmic microwave background | cosmology: observations | atmospheric effects

1. INTRODUCTION

The characterization of the CMB anisotropy is essential for understanding the process of cosmic structure formation (e.g. Hu et al. 1997). If some of the currently popular models prove correct, the anisotropy may be used to strongly constrain cosmological parameters (Jungman et al. 1995, Bond et al. 1998). We report the results from the TOCO 97 campaign of the Mobile Anisotropy Telescope (MAT) experiment.

2. INSTRUMENT

The MAT telescope is essentially the QMAP balloon gondola and instrument (Devlin et al. 1998) mounted on the azimuthal bearing of a surplus Nike Ajax military radar trailer<sup>3</sup>. The receiver has ve cooled corrugated feed horns, one at K<sub>a</sub> band (31 GHz), two at Q band (42 GHz), and two at D band (144 GHz). Each of the K<sub>a</sub> and Q band horns feed two HEMT-based (high electron mobility transistor) amplifiers (Pospieszalski 1992) with one in each polarization. The two D band horns each feed a single SIS detector (Kerr et al. 1993) with one horn in each polarization. This gives a total of eight radiometry channels in the experiment<sup>4</sup>. A Summit mechanical refrigerator cools the HEMT amplifiers to 35 K and the SIS receivers to 4 K.

The telescope optics are similar to those used for three ground-based observations in Saskatoon, SK (Wollack et al. 1997, SK). The feeds underilluminate an ambient temperature 0.85 m  $\phi$ -axis parabolic reflector which in turn underilluminates a computer controlled 1.8 m  $\times$  1.2 m resonant chopping  $\phi$  at mirror. The beams are scanned horizontally across the sky in a 4.6 Hz sinusoidal pattern. The output of the detectors are AC coupled at 0.15 Hz and sampled  $N_c$  times during each chopper cycle. ( $N_c = 80$  for K<sub>a</sub> and Q bands, and  $N_c = 320$  for D band.) The instru-

ment transfer function is essentially flat in frequency and linear in phase between 3 Hz and twice the sample rate. The telescope is inside an aluminum ground screen which is fixed with respect to the receiver and parabola.

The telescope pointing (Table 1) is established through observations of Jupiter and is monitored with two redundant encoders on both the azimuth bearing and on the chopper. The absolute errors in azimuth and elevation are 0:04, and the relative errors are  $< 0:01$ . The surface temperature of the chopper and the rms current required to drive it are monitored. The chopper position was calibrated in the lab and the field. In the analysis, we reject data whenever the rms deviates more than 0:015 from a nominal set of values.

Table 1. TOCO 97 beam characteristics

Feed	Az deg	El deg	meas $10^4$ sr	FWHM avg deg
K <sub>a</sub> 1/2	203.13	41.75	2.75	0.90
Q1/2	206.75	41.85	1.69	0.70
Q3/4	206.70	39.25	1.77	0.72
D1	205.00	40.44	0.183	0.23

3. OBSERVATIONS AND CALIBRATION

Data were taken at a 5200 m site<sup>5</sup> on the side of Cerro Toco (lat. = -22:95 long. = 67:775), near San Pedro de Atacama, Chile, from Oct. 20, 1997 to Dec 15, 1997. The receiver was operational 90% of the available time. For the anisotropy data, the primary optical axis is fixed at az = 204:9, el = 40:5,  $\phi = -62.6$  and the chopper scans with an azimuthal amplitude of 2:96 (8:93 on the sky) as the sky rotates through the beam. The telescope position was not wobbled to the other side of the South Celestial

<sup>1</sup>Princeton University, Physics Department, Jadwin Hall, Princeton, NJ 08544

<sup>2</sup>University of Pennsylvania, Department of Physics and Astronomy, David Rittenhouse Laboratory, Philadelphia, PA 19104

<sup>3</sup>Details of the experiment, synthesis vectors, data, and analysis code may be found at <http://dept.physics.upenn.edu/cmb.html> and <http://pupgg.princeton.edu/~cmb>

<sup>4</sup>HEMT amplifiers have improved considerably since this time (Pospieszalski et al. 1997) and SIS receivers are generally more sensitive than what we achieved. In 1997, one of the D channels and one of the Q channels did not have sufficient sensitivity to warrant a full analysis.

<sup>5</sup>The Cerro Toco site of the Universidad Catolica de Chile was made available through the generosity of Prof. Herman Quintana, Dept. of Astronomy and Astrophysics. It is near the proposed MMA site.

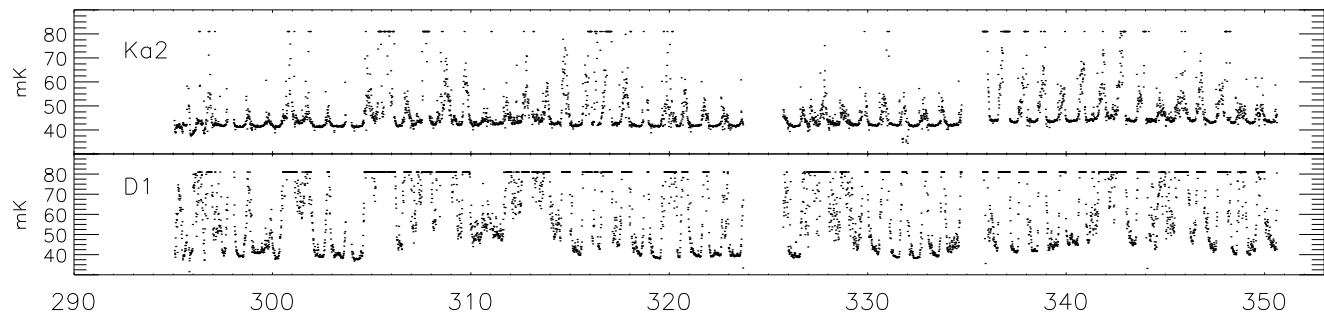


Fig. 1. | The rms detector output in antenna temperature of the  $K_{a2}$  and D1 channels averaged over 0.68 ms (with the chopper running at the nominal amplitude) vs. day of year in 1997. The sky is most stable between 10 PM and 10 AM local time. Similar results from 1998 are consistent with the NRAO opacity measurements.

Pole as for the SK measurements in the North. The rms outputs of the  $K_{a2}$  and D1 channels are shown in Fig. 1.

Jupiter is used to calibrate all channels and map the beams. Its brightness temperature is 152, 160, 170 K for  $K_a$  through D bands respectively (Grin et al. 1986, Ulrich et al. 1981), with an intrinsic calibration error of 5%. We account for the variation in angular diameter.

We also observe Jupiter with multiple relative azimuthal offsets. To convert to thermodynamic units relative to the CMB, we multiply by these numbers by 1.025, 1.045, 1.64 for  $K_a$  through D bands. All anisotropy results are given in thermodynamic temperature.

The variance in the fitted beam solid angle between polarizations and the two QMAP sights is 5% for the  $K_a$  and Q feeds. After determining the beam parameters from a global fit of the clear-weather Jupiter calibrations, the variance in fitted amplitudes is 6% for  $K_a$  through D bands. These errors are uncorrelated between bands. The fitted beam values are strongly correlated with the fitted amplitudes. The error in D is dominated by atmospheric contamination. These sources of calibration error dominate the uncertainty in the passband. The total 1 calibration error is obtained by combining the intrinsic, beam, and measurement errors in quadrature resulting in 10%, 10%, and 11% in  $K_a$  through D respectively.

A thermally-stabilized noise source at  $T_{\text{eff}} = 1$  K is switched on twice for 40 ms every 100 seconds as a relative calibration. The pulse height is correlated to the Jupiter calibrations in the  $K_a$  and Q channels. The variation in detector gain corrected for with these calibration pulses is roughly 5%. No such correction was made for D band.

#### 4. DATA REDUCTION

The reduction is similar to that of the SK experiment (Netterfeld et al. 1997). The raw data,  $d_i$ , are multiplied by  $n$ -pt synthesis vectors,  $SV_{n,i}$  (where  $i$  ranges from 1 to  $N_c$ ) to yield the effective temperature corresponding to a multibeam on the sky,  $H(\theta)$ . For example, we refer to the classic three-lobed beam produced by a "double difference" as the "3-pt harmonic" and write  $t_3 = \sum_{i=1}^{N_c} SV_{3,i} d_i$ . We also record the quadrature signal  $q_n$  (data with chopper sweeping in one direction minus that with the sweeping in the other direction) and fast-dither signal  $f_n^d$  (one value of  $t_n$  minus the subsequent one). For both  $K_{a1/2}$  and Q 3/4 we analyze the unpolar-

ized weighted mean of the combined detector outputs.

The phase of the data relative to the beam position is determined with both Jupiter and observations of the galaxy. We know we are properly phased when the quadrature signal from the galaxy is zero for all harmonics. The relative phases between harmonics agree with those expected from the measured instrument transfer function.

The harmonics are binned according to the right ascension at the center of the chopper sweep. The number of bins depends on the band and harmonic (Table 2). For each night, we compute the sample variance and mean of all the  $t_n$ ,  $q_n$ , and  $f_n^d$  corresponding to a bin. These numbers are appropriately averaged over the campaign and used in the likelihood analysis.

From the raw dataset of 814250 5s averages, we filter out time spent on instrument calibration (6%), celestial calibrations (11%), observations of the galaxy & daytime (53%), and bad pointing (4%). Accounting for overlap, these cut a total of 57%. The data span  $RA = 0$  to 140 ( $b = 55$  to 10).

The data are selected according to the weather by examining each harmonic independently. We first tag 5s averages with a large rms. The untagged data are divided up into 15 minute sections and the rms of the  $t_n$  found. For 15 min sections with rms  $> 1$ , the constituent 5s averages are not used, as well as those of the preceding and succeeding 15 min sections. We ensure that the cut does not bias the statistical weight. As a final cut, nights with less than 4.7 hours of data are excluded. Repeating the analysis with increased cut values produces statistically similar (within 1%) results. The atmosphere cut selects roughly the same sections for  $K_a$  and Q. In the analyses, we discard the 2 and 3-pt data as it is corrupted by atmospheric fluctuations and variable instrumental offsets. If the 4-pt is corrupted, it is at the 1 level and not readily detectable.

The stability of the instrument is assessed through internal consistency checks and with the distribution of the offset of each harmonic. The offset is the average of a night of data after the cuts have been applied (ranges from 5-10 hours) and is of magnitude  $\sim 200$  K with error  $\sim 20$  K. In general, the offset remains constant for a few nights and then jumps 3-5 sigma. The resulting  $\chi^2$  is typically between 4 and 20 for the data over the full campaign and is  $< 1$  for the quadrature signal. In general, a change in offset can have any time scale. The  $q_n$  and  $f_n^d$  are sensitive to  $\tau = 0.25$  s. We also monitor a slow dither (difference of

the subsequent 5 sec averages) with  $\tau = 5$  s and a night-to-night dither with  $\tau = 24$  h. For the final analysis, we delete one seven day section that has a large jump in  $\sigma$ -set. To eliminate the potential effect of slow variations in  $\sigma$ -set, we remove the slope and mean for each night. This is accounted for in the quoted result (both the constraint matrix method, Bond et al. 1998b, and marginalization, Bond et al. 1991 give similar corrections) and does not significantly alter the results over the subtraction of a simple mean. As a test, we have also tried removing quadratic and cubic terms from the  $\sigma$ -set, with no significant changes in the answer.

Each night, different sections of data are removed because of glitches, weather, etc., though all used nights are at least 50% complete. We have tested to ensure that the selected regions do not bias the  $\sigma$ -set and slope removal.

We examined the variations in the power spectrum of the synchronously co-added raw HEMT data, and found no evidence for microphonics. However, a microphonic coupling to the SIS detector was exacerbated after situating the telescope at the site. After filtering, residual signals persisted in the quadrature channels (though not in the fast and slow dithers) and so we report only 95% upper limits for the D channel, specifically  $T_1 < 180$  K at  $\nu = 325$  and  $T_1 < 122$  K at  $\nu = 432$ .

To guard against the possibility that knowledge of previous results biases one's data editing, we set down the selection criteria before the analysis. Outside of an improvement of the calibration, the level of the detected signal did not change significantly over 5 months of investigating the effects of cuts on the data. The primary effect of data editing is to increase the error bar per point and decrease the upper limits of the null tests. Of the 169 null tests (Table 2 plus fast, slow, and night dithers), there are only three failures. When the data are combined into groups of harmonics and bands, there are no failures.

## 5. ANALYSIS AND DISCUSSION

The analysis of the individual harmonics, because the windows are so narrow, essentially corresponds to finding  $T_1^0 = \frac{\sigma^2}{\int W_1^2} = I(W)$ , where  $\sigma^2_{tot}$  is the variance of the data for each harmonic,  $\sigma^2_{inst}$  is the variance due to atmospheric and instrumental noise, and  $I(W) = \frac{\sigma^2_{tot}}{\int W_1^2}$ .  $W_1$  is the window function, as defined in Bond 1996. The full likelihood analysis provides a formal way of determining  $T_1$  that includes correlations and gives the correct error bar in the low signal-to-noise limit.

The error in  $I(W)$  is determined from the scatter in the beam values. We find  $I(W) = I(W) \pm 0.01$ . The mean variance,  $\sigma^2_{inst}$ , is determined directly from the uncertainties in each bin. If these uncertainties are somehow biased, the results of the simple test and full likelihood will be biased. We examine the distribution of all the data for each harmonic from all the nights after removing the mean value of each sky bin. The width of this distribution agrees with the mean error bar indicating that the error per point is not biased. Also, the ratio of the error bars between harmonics agrees with the analytic calculation.

In the full analysis (Fig. 2), we include all known correlations inherent in the observing strategy. From the data,

we determine the correlations between harmonics due to the atmosphere, detector noise, and non-orthogonality of the synthesis vectors. The correlation coefficients between bands due to atmosphere are of order 0.05. We also examine the autocorrelation function of the data for a single harmonic to ensure that atmospheric fluctuations do not correlate one bin to the next. The quoted results are insensitive to the precise values of the off-diagonal terms of the covariance matrix.

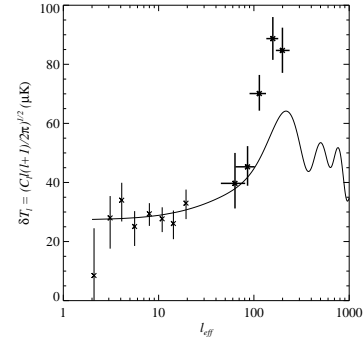


FIG. 2. Combined analysis of data in Table 2. The values are  $(l; T_1 [K]) = (63^{+18}_{-18}; 40^{+10}_{-9}), (86^{+16}_{-22}; 45^{+7}_{-6}), (114^{+20}_{-24}; 70^{+6}_{-6}), (158^{+22}_{-23}; 89^{+7}_{-7}), (199^{+38}_{-29}; 85^{+8}_{-8})$ . Error bars are  $\sqrt{1 \text{ statistical}}$ ; calibration error is not included. The COBE/DMR points are from Tegmark 1997. The solid curve is standard CDM ( $\omega_b = 0.05, h = 0.5$ ).

These results are similar to previous results obtained with this technique (SK) though the experiment was done with different optics, a different receiver, a different primary calibrator, largely different analysis code, and observed a different part of the sky. Though we have not correlated our data with templates of foreground emission, the foreground contribution is known to be small at these frequencies and galactic latitudes (Coble et al. 1999, de Oliveira-Costa et al. 1997). In addition, the fluctuations in  $K_a$  and  $Q$  bands are comparable, suggesting the frequency spectrum of the fluctuations is close to thermal. The full analysis has been repeated after deleting each 15 section of data in RA, indicating that the signal does not arise from one region. (Our scan passes near, but misses, the LMC.) Future work will address the precise level of contamination.

We gratefully acknowledge the insights and help from Dave Wilkinson, Norm Jarosik, Ray Blundell, Angel Otárola, Herman Quintana, Robert Caldwell, Ted Grith, Bernard Jones, and Harvey Chapman. The experiment would not have been possible without NRAO's site monitoring and detector development. We also thank Lucent Technologies for donating the radar trailer. This work was supported by an NSF NYI award, a Cottrell Award from the Research Corporation, a David and Lucile Packard Fellowship (to LP), a NASA GSRP fellowship to AM, an NSF graduate fellowship to MN, NSF grants PHY-9222952, PHY-9600015, AST-9732960, and the University of Pennsylvania. The data will be made public upon publication of this Letter.

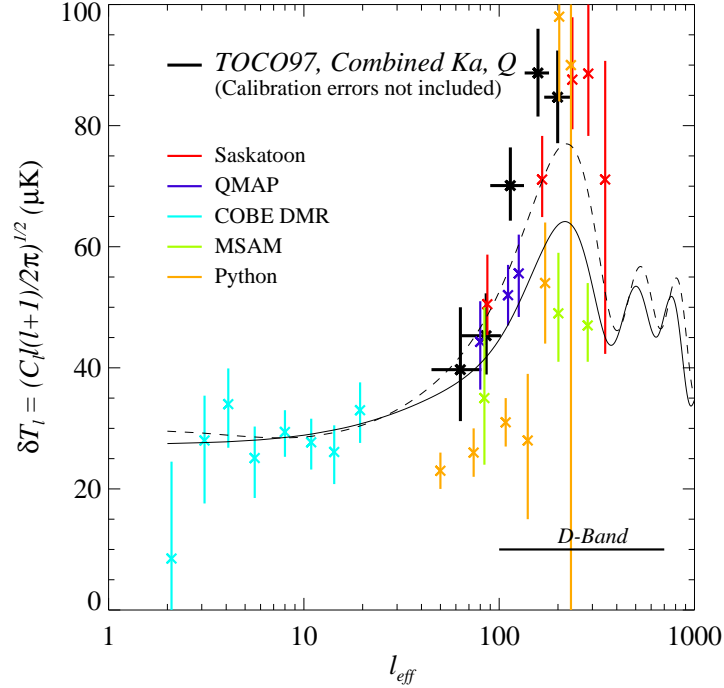
## REFERENCES

- Bond, J. R., Efstathiou, G., Lubin, P. M., & Meinholt, P. R. 1991, *Phys. Rev. Lett.*, 66, 2179
- Bond, J. R. 1996 Theory and Observations of the Cosmic Microwave Background Radiation, in "Cosmology and Large-Scale Structure," Les Houches Session LX, August 1993, ed. R. Schaefer, Elsevier Science Press
- Bond, J. R., Efstathiou, G., & Tegmark, M. 1998, *MNRAS*, 50, L33
- Bond, J. R., Jaffe, A. H., & Knox, L. 1998, *Phys. Rev. D*, 57, 2117
- Coble, K., et al. 1999, astro-ph/9902195
- de Oliveira-Costa, A., Kogut, A., Devlin, M. J., Netterfeld, C. B., Page, L. A., & Wollack, E. J. 1997 *ApJ*, 482, L17
- Devlin, M. J., de Oliveira-Costa, A., Herbig, T., Miller, A. D., Netterfeld, C. B., Page, L., & Tegmark, M. 1998, *ApJ*, 509, L73
- Griest, M. J., Ade, A. R., Orton, G. S., Robson, E. I., Gear, W. K., Nolt, I. G., & Radostitz, J. V. 1986, *Icarus*, 65, 244
- Hu, W., Sugiyama, N., & Silk, J. 1997, *Nature*, 386, 37
- Jungmann, G., Kamionkowski, M., Kosowsky, A., & Spergel, D. N. 1995, *Phys. Rev. D*, 54, 1332
- Netterfeld, C. B., Devlin, M. J., Jarosik, N., Page, L., & Wollack, E. J. 1997, *ApJ*, 474, 47
- Kerr, A. R., Pan, S.-K., Lichtenberger, A. W., & Lloyd, F. L. 1993, Proceedings of the Fourth International Symposium on Space Terahertz Technology, 1
- Pospieszalski, M. W. 1992, *IEEE MTT-S Digest*, 1369; also see Pospieszalski, M. W. et al. 1994, *IEEE MTT-S Digest*, 1345
- Pospieszalski, M. W. 1997, *Microwave Background Anisotropies* (Ed. Frontiers, ed. Bouchet et al.), 23
- Tegmark, M., 1997, *Phys. Rev. D*, 55, 5895
- Ulich, B. L. 1981, *AJ*, 86, 1619
- Wollack, E. J., Devlin, M. J., Jarosik, N. J., Netterfeld, C. B., Page, L., & Wilkinson, D. 1997, *ApJ*, 476, 440

Table 2  
TOCO 97 Angular Spectrum

Band/SV	$\nu_e^a$	$T_{\nu}^b$ K	$N_{bins}^c$	$T_{\nu}^0$ K	$T_{tot}^b$ K	$T_{inst}^b$ K	$\frac{P}{I(W)}$	$(A-B)/2^b$ K	$Q_{quad}, Q_n^b$ K	$(H1-H2)/2^b$ K
K a 1/2										
4pt	$63^{+17}_{-18}$	$35^{+13}_{-9}$	48 (16)	32	33	20	0.84	< 27	< 30	< 29
5pt	$86^{+16}_{-21}$	$52^{+11}_{-8}$	64 (28)	49	40	21	0.71	< 21	< 32	< 29
6pt	$107^{+16}_{-21}$	$71^{+12}_{-10}$	96 (42)	69	52	27	0.65	< 32	< 31	< 35
7pt	$127^{+16}_{-22}$	$93^{+15}_{-14}$	96 (41)	90	57	27	0.55	< 35	< 37	< 30
8pt	$145^{+18}_{-20}$	$103^{+16}_{-13}$	128 (55)	102	63	34	0.52	< 51	< 46	< 43
9pt	$165^{+18}_{-20}$	$65^{+16}_{-17}$	128 (54)	59	47	38	0.46	< 63	< 72	< 66
10pt	$182^{+21}_{-17}$	$67^{+20}_{-23}$	192 (82)	70	60	51	0.44	< 68	< 69	< 60
11pt	$192^{+30}_{-8}$	< 119	192 (82)	67	65	58	0.42	< 91	< 83	< 86
12pt	$215^{+27}_{-11}$	$128^{+30}_{-33}$	192 (82)	127	83	68	0.37	< 150	< 86	< 76
Q 1										
4pt	$63^{+17}_{-18}$	$57^{+18}_{-13}$	48 (20)	51	53	31	0.83		< 44	< 47
5pt	$87^{+16}_{-22}$	$40^{+14}_{-14}$	64 (28)	34	40	33	0.71		< 36	< 47
6pt	$110^{+15}_{-24}$	$56^{+14}_{-13}$	96 (42)	52	52	40	0.65		< 45	$+45_{-14}$
7pt	$131^{+14}_{-25}$	$81^{+19}_{-16}$	96 (42)	77	59	41	0.55		< 65	< 53
8pt	$151^{+15}_{-25}$	$86^{+17}_{-17}$	128 (55)	79	66	50	0.53		< 45	< 64
9pt	$172^{+14}_{-26}$	$93^{+23}_{-23}$	128 (55)	89	68	54	0.47		< 82	< 72
10pt	$191^{+16}_{-24}$	< 115	192 (84)	31	75	74	0.47		< 105	< 92
11pt	$203^{+24}_{-17}$	< 117	192 (84)	44	80	78	0.44		< 103	< 83
12pt	$221^{+25}_{-15}$	< 169	192 (84)	91	91	84	0.40		< 138	< 119
13pt	$245^{+21}_{-20}$	< 130	192 (84)		84	92	0.37		< 163	< 164
14pt	$267^{+20}_{-23}$	< 202	256 (112)	123	123	114	0.37		< 183	< 188
Q 3/4										
5pt	$83^{+15}_{-20}$	$47^{+17}_{-13}$	64 (17)	43	39	24	0.73	$31^{+10}_{-8}$	< 50	< 58
6pt	$106^{+14}_{-23}$	$61^{+18}_{-13}$	96 (22)	55	46	28	0.66	< 27	< 34	< 61
7pt	$125^{+14}_{-23}$	$72^{+16}_{-12}$	96 (35)	71	50	30	0.56	< 29	< 57	< 31
8pt	$145^{+14}_{-23}$	$115^{+19}_{-15}$	128 (45)	109	68	35	0.54	< 26	< 38	< 60
9pt	$165^{+14}_{-24}$	$72^{+24}_{-21}$	128 (29)	65	48	37	0.48	< 43	< 97	< 84
10pt	$184^{+15}_{-23}$	$87^{+19}_{-19}$	192 (70)	86	63	48	0.47	< 68	< 45	< 52
11pt	$196^{+22}_{-17}$	$90^{+27}_{-26}$	192 (54)	84	65	53	0.44	< 64	< 78	< 75
12pt	$212^{+25}_{-13}$	$100^{+29}_{-27}$	192 (65)	97	69	57	0.40	< 70	< 129	< 84
13pt	$236^{+20}_{-19}$	< 157	192 (56)	80	71	65	0.37	< 107	< 121	< 153
14pt	$258^{+18}_{-23}$	$119^{+36}_{-38}$	256 (103)	119	91	80	0.36	< 116	< 137	< 103

Note. (a) The range for  $\nu_e$  denotes the range for which the window function exceeds  $e^{-1}$  times the peak value. (b) The error on  $T_{\nu} = [(\nu + 1)C_{\nu}]^{1/2}$  is comprised of experimental uncertainty and sample variance. The calibration error is not included. These values are not statistically independent: harmonic numbers differing by 2 are correlated at the 0.35 level. For all harmonics, the sample variance ( $\sigma^2 = \frac{P}{2N_{bins}}$ ) is  $\approx 7$  K. The values for  $T_{tot}$  and  $T_{inst}$  have not been divided by  $\frac{P}{I(W)}$ . The " $<$ " indicates a 95% upper limit.  $(A-B)/2$  is the difference in polarizations and  $(H1-H2)/2$  is the first half minus the second half. (c) The number of bins on the sky followed by, in parentheses, the number used in the analysis due to the galactic/atmosphere cut.



Angular spectrum from the *SK*, *QMAP*, and *TOCO97* experiments. The *SK* data from Netterfield *et al.* (1997, ApJ, 474:47) and Wollack *et al.* (1997, ApJ 476:440) have been recalibrated according to the Mason *et al.* (1997, astro-ph/9903383), leading to an increase of 5%, and reduced according to the foreground contribution in de Oliveira-Costa *et al.* (1997, ApJL, 482:L17), leading to a reduction of 2%. The foreground reduction was applied uniformly. Because the *SK* data are primarily at 40 GHz, the Mason *et al.* results must be extrapolated. In addition, uncertainty in the measured passband, measurement uncertainty, and beam uncertainty, must be taken into account. This leads to a  $1\sigma$  calibration error of 11%. The *QMAP* data are the same as those reported in de Oliveira-Costa *et al.* (1998, ApJL, 509:L78) and have an average calibration error of 12%, the correction for foreground emission is  $\approx 2\%$  (de Oliveira-Costa *et al.* 1999, *in prep*), though has not yet been precisely determined and so is not included. Both *SK* and *QMAP* are calibrated with respect to Cas-A. The *TOCO97* data, which have a calibration error of 10%, are calibrated with respect to Jupiter. A foreground contribution, which is expected to be small, has not been subtracted. When calibration errors are included, all three independent experiments agree. Two cosmological models are shown for reference. The lower is “standard CDM” ( $\Omega_0 = 1$ ,  $\Omega_B = 0.05$ ,  $h = 0.5$ ); the upper one is a current “concordance model” (Wang *et al.* 1999 astro-ph/9901388) with  $\Omega_0 = 0.33$ ,  $\Omega_B = 0.041$ ,  $\Omega_\Lambda = 0.67$ , and  $h = 0.65$ . For *COBE/DMR* we use the results from Tegmark. We also plot recent results from MSAM (Wilson *et al.* 1999 astro-ph/9902047) and from Python (Coble *et al.* 1999 astro-ph/9902195)